High Statistics Measurement of the Positron Fraction in Primary Cosmic Rays of 0.5–500 GeV with the Alpha Magnetic Spectrometer on the International Space Station

L. Accardo,[34] M. Aguilar,[26] D. Aisa,[34,35] B. Alpat,[34] A. Alvino,[34] G. Ambrosi,[34] K. Andeen,[22] L. Arruda,[24] N. Attig,[21] P. Azzarello,[34,16,a] A. Bachlechner,[1] F. Barao,[24] A. Barrau,[17] L. Barrin,[15] A. Bartoloni,[39] L. Basara,[3,38] M. Battarbee,[45] R. Battiston,[38,b] J. Bazo,[34,c] U. Becker,[9] M. Behlmann,[9] B. Beischer,[1] J. Berdugo,[26] B. Bertucci,[34,35] G. Bigongiari,[36,37] V. Bindi,[19] S. Bizzaglia,[34] M. Bizzarri,[34,35] G. Boella,[29,30] W. de Boer,[22] K. Bollweg,[20] V. Bonnivard,[17] B. Borgia,[39,40] S. Borsini,[34] M. J. Boschini,[29] M. Bourquin,[16] J. Burger,[9] F. Cadoux,[16] X. D. Cai,[9] M. Capell,[9] S. Caroff,[3] G. Carosi,[9,d] J. Casaus,[26] V. Cascioli,[34] G. Castellini,[14] I. Cernuda,[26] D. Cerreta,[34,35] F. Cervelli,[36] M. J. Chae,[41] Y. H. Chang,[10] A. I. Chen,[9] H. Chen,[9] G. M. Cheng,[6] H. S. Chen,[6] L. Cheng,[42] A. Chikanian,[33,e] H. Y. Chou,[10] E. Choumilov,[9] V. Choutko,[9] C. H. Chung,[1] F. Cindolo,[7,8] C. Clark,[20] R. Clavero,[23] G. Coignet,[3] C. Consolandi,[19] A. Contin,[7,8] C. Corti,[19] B. Coste,[38] Z. Cui,[42] M. Dai,[5] C. Delgado,[26] S. Della Torre,[29] M. B. Demirköz,[2] L. Derome,[17] S. Di Falco,[36] L. Di Masso,[34,35] F. Dimiccoli,[38] C. Díaz,[26] P. von Doetinchem,[19] W. J. Du,[42] M. Duranti,[34] D. D'Urso,[34] A. Eline,[9] F. J. Eppling,[9] T. Eronen,[45] Y. Y. Fan,[44,f] L. Farnesini,[34] J. Feng,[3,g] E. Fiandrini,[34,35] A. Fiasson,[3] E. Finch,[33] P. Fisher,[9] Y. Galaktionov,[9] G. Gallucci,[36,15] B. García,[26] R. García-López,[23] H. Gast,[1] I. Gebauer,[22] M. Gervasi,[29,30] A. Ghelfi,[17] W. Gillard,[10] F. Giovacchini,[26] P. Goglov,[9] J. Gong,[32] C. Goy,[3] V. Grabski,[27] D. Grandi,[29] M. Graziani,[34,15] C. Guandalini,[7,8] I. Guerri,[36,37] K. H. Guo,[18] D. Haas,[16,h] M. Habiby,[16] S. Haino,[10,44] K. C. Han,[25] Z. H. He,[18] M. Heil,[22,9] R. Henning,[9,i] J. Hoffman,[10] T. H. Hsieh,[9] Z. C. Huang,[18] C. Huh,[13] M. Incagli,[36] M. Ionica,[34] W. Y. Jang,[13] H. Jinchi,[25] K. Kanishev,[38] G. N. Kim,[13] K. S. Kim,[13] Th. Kirn,[1] R. Kossakowski,[3] O. Kounina,[9] A. Kounine,[9] V. Koutsenko,[9] M. S. Krafczyk,[9] S. Kunz,[22] G. La Vacca,[29,15] E. Laudi,[34,35,j] G. Laurenti,[7,8] I. Lazzizzera,[38] A. Lebedev,[9] H. T. Lee,[44] S. C. Lee,[44] C. Leluc,[16] G. Levi,[7,8] H. L. Li,[44,k] J. Q. Li,[32] Q. Li,[32] Q. Li,[9,l] T. X. Li,[18] W. Li,[4] Y. Li,[16,g] Z. H. Li,[6] Z. Y. Li,[44,g] S. Lim,[41] C. H. Lin,[44] P. Lipari,[39] T. Lippert,[21] D. Liu,[44] H. Liu,[32] M. Lolli,[7,8] T. Lomtadze,[36] M. J. Lu,[38,m] Y. S. Lu,[6] K. Luebelsmeyer,[1] F. Luo,[42] J. Z. Luo,[32] S. S. Lv,[18] R. Majka,[33] A. Malinin,[12] C. Mañá,[26] J. Marín,[26] T. Martin,[20] G. Martínez,[26] N. Masi,[7,8] F. Massera,[7,8] D. Maurin,[17] A. Menchaca-Rocha,[27] Q. Meng,[32] D. C. Mo,[18] B. Monreal,[9,n] L. Morescalchi,[36,o] P. Mott,[20] M. Müller,[1] J. Q. Ni,[18] N. Nikonov,[22] F. Nozzoli,[34,c] P. Nunes,[24] A. Obermeier,[1] A. Oliva,[26] M. Orcinha,[24] F. Palmonari,[7,8] C. Palomares,[26] M. Paniccia,[16] A. Papi,[34] M. Pauluzzi,[34,35] E. Pedreschi,[36] S. Pensotti,[29,30] R. Pereira,[24,19] R. Pilastrini,[7,8] F. Pilo,[36] A. Piluso,[34,35] C. Pizzolotto,[34,c] V. Plyaskin,[9] M. Pohl,[16] V. Poireau,[3] E. Postaci,[2] A. Putze,[3] L. Quadrani,[7,8] X. M. Qi,[18] P. G. Rancoita,[29] D. Rapin,[16] J. S. Ricol,[17] I. Rodríguez,[26] S. Rosier-Lees,[3] L. Rossi,[15] A. Rozhkov,[9] D. Rozza,[29] G. Rybka,[9,p] R. Sagdeev,[11] J. Sandweiss,[33] P. Saouter,[16] C. Sbarra,[7,8] S. Schael,[1] S. M. Schmidt,[21] D. Schuckardt,[22] A. Schulz von Dratzig,[1] G. Schwering,[1] G. Scolieri,[34] E. S. Seo,[12] B. S. Shan,[4] Y. H. Shan,[4] J. Y. Shi,[32] X. Y. Shi,[9,q] Y. M. Shi,[43] T. Siedenburg,[1] D. Son,[13] F. Spada,[39] F. Spinella,[36] W. Sun,[9] W. H. Sun,[9,r] M. Tacconi,[29,30] C. P. Tang,[18] X. W. Tang,[6] Z. C. Tang,[6] L. Tao,[3] D. Tescaro,[23] Samuel C. C. Ting,[9] S. M. Ting,[9] N. Tomassetti,[17] J. Torsti,[45] C. Türkoğlu,[2] T. Urban,[20] V. Vagelli,[22] E. Valente,[39,40] C. Vannini,[36] E. Valtonen,[45] S. Vaurynovich,[9] M. Vecchi,[3,s] M. Velasco,[26] J. P. Vialle,[3] V. Vitale,[34,c] G. Volpini,[28] L. Q. Wang,[42] Q. L. Wang,[5] R. S. Wang,[43] X. Wang,[9] Z. X. Wang,[18] Z. L. Weng,[9] K. Whitman,[19] J. Wienkenhöver,[1] H. Wu,[32] K. Y. Wu,[44] X. Xia,[26,k] M. Xie,[9,l] S. Xie,[43] R. Q. Xiong,[32] G. M. Xin,[42] N. S. Xu,[18] W. Xu,[6,9] Q. Yan,[6] J. Yang,[41] M. Yang,[6] Q. H. Ye,[43] H. Yi,[32] Y. J. Yu,[5] Z. Q. Yu,[6] S. Zeissler,[22] J. H. Zhang,[32] M. T. Zhang,[18] X. B. Zhang,[18] Z. Zhang,[18] Z. M. Zheng,[4] F. Zhou,[9,t] H. L. Zhuang,[6] V. Zhukov,[1] A. Zichichi,[7,8] N. Zimmermann,[1] P. Zuccon,[9] and C. Zurbach[31]

(AMS Collaboration)

[1]*I. Physics Institute and JARA-FAME, RWTH Aachen University, D–52056 Aachen, Germany*[u]
[2]*Department of Physics, Middle East Technical University, METU, 06800 Ankara, Turkey*[v]
[3]*Laboratoire d'Annecy–Le–Vieux de Physique des Particules, LAPP, IN2P3/CNRS and Université de Savoie, F–74941 Annecy–le–Vieux, France*
[4]*Beihang University, BUAA, Beijing 100191, China*
[5]*Institute of Electrical Engineering, IEE, Chinese Academy of Sciences, Beijing 100080, China*
[6]*Institute of High Energy Physics, IHEP, Chinese Academy of Sciences, Beijing 100039, China*[w]
[7]*INFN-Sezione di Bologna, I-40126 Bologna, Italy*[x]
[8]*Università di Bologna, I-40126 Bologna, Italy*
[9]*Massachusetts Institute of Technology, MIT, Cambridge, Massachusetts 02139, USA*
[10]*National Central University, NCU, Chung–Li, Tao Yuan 32054, Taiwan*[y]

[11]East–West Center for Space Science, University of Maryland, College Park, Maryland 20742, USA
[12]IPST, University of Maryland, College Park, Maryland 20742, USA
[13]CHEP, Kyungpook National University, 702–701 Daegu, Korea[z]
[14]CNR–IROE, I-50125 Firenze, Italy
[15]European Organization for Nuclear Research, CERN, CH–1211 Geneva 23, Switzerland
[16]DPNC, Université de Genève, CH–1211 Genève 4, Switzerland
[17]Laboratoire de Physique Subatomique et de Cosmologie, LPSC, Université Grenoble–Alpes, CNRS/IN2P3, F–38026 Grenoble, France
[18]Sun Yat–Sen University, SYSU, Guangzhou 510275, China
[19]Physics and Astronomy Department, University of Hawaii, 2505 Correa Road, WAT 432, Honolulu, Hawaii 96822, USA
[20]NASA, National Aeronautics and Space Administration, Johnson Space Center, JSC, and Jacobs-Sverdrup, Houston, Texas 77058, USA
[21]Jülich Supercomputing Centre and JARA-FAME, Research Centre Jülich, D–52425 Jülich, Germany[A]
[22]Institut für Experimentelle Kernphysik, Karlsruhe Institute of Technology, KIT, D–76128 Karlsruhe, Germany[B]
[23]Instituto de Astrofísica de Canarias, IAC, E–38205 La Laguna, Tenerife, Spain
[24]Laboratório de Instrumentação e Física Experimental de Partículas, LIP, P–1000 Lisboa, Portugal
[25]National Chung–Shan Institute of Science and Technology, NCSIST, Longtan, Tao Yuan 325, Taiwan
[26]Centro de Investigaciones Energéticas, Medioambientales y Tecnológicas, CIEMAT, E–28040 Madrid, Spain[C]
[27]Instituto de Física, Universidad Nacional Autónoma de México, UNAM, México D.F. 01000, México[D]
[28]INFN-Sezione di Milano and Università di Milano, I-20090 Milano, Italy
[29]INFN-Sezione di Milano–Bicocca, I-20126 Milano, Italy[x]
[30]Università di Milano–Bicocca, I-20126 Milano, Italy
[31]Laboratoire Univers et Particules de Montpellier, LUPM, IN2P3/CNRS and Université de Montpellier II, F–34095 Montpellier, France
[32]Southeast University, SEU, Nanjing 210096, China
[33]Physics Department, Yale University, New Haven, Connecticut 06520, USA
[34]INFN-Sezione di Perugia, I-06100 Perugia, Italy[x]
[35]Università di Perugia, I-06100 Perugia, Italy
[36]INFN-Sezione di Pisa, I-56100 Pisa, Italy[x]
[37]Università di Pisa, I-56100 Pisa, Italy
[38]INFN–TIFPA and Università di Trento, I-38123 Povo, Trento, Italy[x]
[39]INFN-Sezione di Roma 1, I-00185 Roma, Italy[x]
[40]Università di Roma La Sapienza, I-00185 Roma, Italy
[41]Department of Physics, Ewha Womans University, Seoul 120-750, Korea[E]
[42]Shandong University, SDU, Jinan, Shandong 250100, China
[43]Shanghai Jiaotong University, SJTU, Shanghai 200030, China
[44]Institute of Physics, Academia Sinica, Nankang, Taipei 11529, Taiwan[y]
[45]Space Research Laboratory, Department of Physics and Astronomy, University of Turku, FI–20014 Turku, Finland

(Received 18 July 2014; revised manuscript received 6 August 2014; published 18 September 2014)

A precision measurement by AMS of the positron fraction in primary cosmic rays in the energy range from 0.5 to 500 GeV based on 10.9 million positron and electron events is presented. This measurement extends the energy range of our previous observation and increases its precision. The new results show, for the first time, that above ~200 GeV the positron fraction no longer exhibits an increase with energy.

DOI: 10.1103/PhysRevLett.113.121101 PACS numbers: 96.50.sb, 95.35.+d, 95.85.Ry, 98.70.Sa

Over the last two decades, there has been a strong interest in the cosmic ray positron fraction in both particle physics and astrophysics [1]. The positron fraction is defined as the ratio of the positron flux to the combined flux of positrons and electrons. The first results from the Alpha Magnetic Spectrometer (AMS) on the positron fraction were reported in [2]. They generated widespread interest [3]. In this Letter, we report new results based on all the data collected during 30 months of AMS operations on the International Space Station (ISS), from 19 May 2011 to 26 November 2013. Because of the excellent and steady performance of the detector, and an increase of the data sample by a factor of 1.7, the measurement of the positron fraction is extended up to 500 GeV with improved precision.

AMS detector.—The layout of the AMS-02 detector [4] is shown in Fig. 1. It consists of nine planes of precision silicon tracker with two outer planes, 1 and 9, and the inner tracker, planes 2 to 8 [5]; a transition radiation detector (TRD) [6]; four planes of time of flight (TOF) counters [7]; a permanent magnet [8]; an array of anticoincidence counters (ACC) [9], inside the magnet bore; a ring imaging

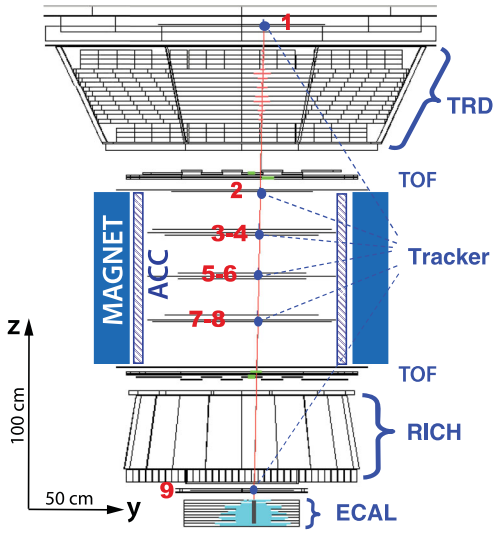

FIG. 1 (color). A 369 GeV positron event as measured by the AMS detector on the ISS in the bending (y-z) plane. Tracker planes 1 to 9 measure the particle charge, sign, and momentum. The TRD identifies the particle as $e^{\pm}$. The TOF measures the absolute charge value to be one and ensures that the particle is downward going. The RICH independently measures the charge and velocity. The ECAL measures the 3D shower profile, independently identifies the particle as an $e^{\pm}$, and measures its energy. A positron is identified by (1) positive rigidity in the tracker, (2) an $e^{\pm}$ signal in the TRD, (3) an $e^{\pm}$ signal in the ECAL, and (4) the matching of the ECAL shower energy and axis with the momentum measured with the tracker and magnet. Note: the 3D ECAL has nine superlayers along the z axis with fibers in alternating directions. In the (y-z) plane the wider rectangles display the width of the shower in five superlayers and the narrower rectangles display the energy deposition per layer in the other four alternating superlayers. The shower axis is defined from the 3D shower shape.

Čerenkov detector (RICH) [10]; and an electromagnetic calorimeter (ECAL) [11]. The figure also shows a high energy positron of 369 GeV recorded by AMS. AMS operates without interruption on the ISS and is monitored continuously from the ground.

The timing, location, and attitude of AMS are determined by a combination of global positioning system units affixed to AMS and to the ISS. The AMS coordinate system is concentric with the center of the magnet. The x axis is parallel to the main component of the magnetic field and the z axis points vertically. The (y-z) plane is the bending plane. The maximum detectable rigidity over tracker planes 1 to 9, a lever arm of 3 m, is $\sim$2 TV. Detector performance, described in detail in [2,4], is steady over time.

Three main detectors provide clean and redundant identification of positrons and electrons with independent suppression of the proton background. These are the TRD (above the magnet), the ECAL (below the magnet), and the tracker. The TRD and the ECAL are separated by the magnet and the tracker. This ensures that most of the secondary particles produced in the TRD and in the upper TOF planes are swept away and do not enter into the ECAL. Events with large angle scattering are also rejected by a quality cut on the measurement of the trajectory using the tracker. The matching of the ECAL energy, E, and the momentum measured with the tracker, p, greatly improves the proton rejection.

To differentiate between $e^{\pm}$ and protons in the TRD, signals from the 20 layers of proportional tubes are combined in a TRD estimator formed from the ratio of the log-likelihood probability of the $e^{\pm}$ hypothesis to that of the proton hypothesis in each layer. The proton rejection power of the TRD estimator at 90% $e^{\pm}$ efficiency measured on orbit is 10^3 to 10^4 [2].

To cleanly identify electrons and positrons in the ECAL, an estimator, based on a boosted decision tree algorithm [12], is constructed using the 3D shower shape in the ECAL. The proton rejection power of the ECAL estimator reaches 10^4 when combined with the energy-momentum matching requirement $E/p > 0.75$ [2].

The entire detector has been extensively calibrated in a test beam at CERN with e^+ and e^- from 10 to 290 GeV/c, with protons at 180 and 400 GeV/c, and with $\pi^{\pm}$ from 10 to 180 GeV/c which produce transition radiation equivalent to protons up to 1.2 TeV/c. In total, measurements with 18 different energies and particles at 2000 positions were performed [2].

Data sample and analysis procedure.—Over 41 billion events have been analyzed following the general procedure presented in [2]. Optimization of all reconstruction algorithms was performed using the test beam data. Several corrections are applied to the data to ensure long term stability of the absolute scales in the constantly varying on-orbit environment. These corrections are performed using specific samples of particles, predominantly protons. They include off-line calibrations of the amplitude response of TRD, TOF, tracker, and ECAL electronic channels. These calibrations are performed every 1/4 of an orbit with the exception of the alignment of the outer tracker planes 1 and 9 which is performed every two minutes. The stability of the electronics response is ensured by onboard calibrations of all channels every half-orbit ($\sim$46 min). The corrections also include the alignment of all the AMS detectors and the temperature correction of the magnetic field strength.

Monte Carlo simulated events are produced using a dedicated program developed by AMS based on GEANT-4.9.4 [13]. This program simulates electromagnetic and hadronic interactions of particles in the materials of AMS and generates detector responses. The digitization of the signals, including those of the trigger, is simulated according to the measured characteristics of the electronics. The digitized signals then undergo the same reconstruction as used for the data. The Monte Carlo samples used in the

present analysis have sufficient statistics such that they do not contribute to the errors.

Events are selected by requiring a track in the TRD and in the tracker, a cluster of hits in the ECAL, and a measured velocity $\beta \sim 1$ in the TOF consistent with a downward-going $|Z| = 1$ particle. To reject the bulk of the remaining protons, an energy-dependent cut on the ECAL estimator is applied. To reject secondary positrons and electrons produced by the interaction of primary cosmic rays with the atmosphere [14], the energy measured with the ECAL is required to exceed, by a factor of 1.2, the maximum Størmer cutoff [15] for either a positron or electron at the geomagnetic location where the particle was detected and at any angle within the acceptance.

The resulting acceptance for electrons and positrons is identical and nearly constant over the range from 3 to 500 GeV. It takes into account the geometric acceptance, the selection efficiency, and the trigger efficiency. Any charge asymmetry in the azimuthal angular acceptance, present only below 3 GeV, is accounted for in the systematic errors. The integrated acceptance for positrons and electrons is the same within our statistics and cancels in the fraction.

The positron fraction is determined in energy bins as measured with the ECAL. The set of bins used in our previous publication is extended, consistent with the energy resolution and available statistics. Migration of the signal events to neighboring bins has a negligible contribution to the systematic errors.

Compared to our previous publication [2], systematic errors have decreased with increasing statistics in the high energy region. As other uncertainties have decreased, the contribution of the absolute energy scale uncertainty became noticeable. The energy scale is verified by using minimum ionizing particles and the ratio E/p. These results are compared with the test beam values where the beam energy is known to high precision. This comparison limits the uncertainty of the absolute energy scale to 2% in the range covered by the beam test results, 10–290 GeV. It increases to 5% at 0.5 GeV and to 3% at 500 GeV. This results in a negligible contribution to the total systematic error, except below 5 GeV, where it dominates.

In each energy bin, the two-dimensional reference spectra for $e^{\pm}$ and the background are fit to data in the [TRD estimator–$\log(E/p)$] plane by varying the normalizations of the signal and the background. This method provides a data-driven control of the dominant systematic uncertainties by combining the redundant and independent TRD, ECAL, and tracker information. The reference spectra are determined from high statistics electron and proton data samples selected using tracker and ECAL information including charge sign, track-shower axis matching, and the ECAL estimator. The purity of each reference spectrum is verified using Monte Carlo simulation.

The fit is performed simultaneously for the positive and negative rigidity data samples in each energy bin yielding the number of positrons, the number of electrons, the number of protons, and the amount of charge confusion, where charge confusion is defined as the fraction of electrons or positrons reconstructed with a wrong charge sign. Charge confusion is discussed further below.

From the bin-by-bin fits, the sample contains 10.9×10^6 primary positrons and electrons and 3.50×10^6 protons. A total of 0.64×10^6 events are identified as positrons.

There are several systematic uncertainties. In addition to the energy scale, bin-to-bin migration, and asymmetric acceptance of e^+ and e^- below 3 GeV discussed above, there are also the systematic uncertainties from event selection, charge confusion, and the reference spectra.

To evaluate the systematic uncertainty related to event selection, the complete analysis is repeated in every energy bin over 1000 times with different cut values, such that the selection efficiency varies up to 30%. The distribution of the positron fraction resulting from these 1000 analyses contains both statistical and systematic effects. The difference between the width of this distribution from data and from Monte Carlo simulation quantifies this systematic uncertainty.

Two sources of charge confusion dominate. The first source is related to the finite resolution of the tracker and multiple scattering. It is mitigated by the E/p matching and quality cuts of the trajectory measurement including the track χ^2, charge measured in the tracker, and charge measured in the TOF. The second source is related to the production of secondary tracks along the path of the primary $e^{\pm}$ in the tracker. It was studied using control data samples of electron events where the ionization in the lower TOF counters corresponds to at least two traversing particles. Both sources of charge confusion are found to be well reproduced by the Monte Carlo simulation and their reference spectra are derived from the Monte Carlo simulation. The systematic uncertainties due to these two effects are obtained by varying the background normalizations within the statistical limits and comparing the results with the Monte Carlo simulation. They were examined in each energy bin.

The proton contamination in the region populated by positrons is small. It is accurately measured using the TRD estimator. The amount of proton contamination has a negligible contribution to the statistical error.

The systematic error associated with the uncertainty of the data derived reference spectra arises from their finite statistics. It is measured by varying the shape of the reference spectra within the statistical uncertainties. Its contribution to the overall error is small compared to the statistical uncertainty of data and is included in the total systematic error.

Results and conclusions.—The measured positron fraction is presented in Table I as a function of the energy at the

TABLE I. Positron fraction as a function of energy. The number of positrons, N_{e^+}, is corrected for charge confusion. Errors due to: statistical error (stat.), acceptance asymmetry (acc.), event selection (sel.), energy scale and bin-to-bin migration (mig.), reference spectra (ref.), charge confusion (c.c.), and total systematic error (syst.).

Energy [GeV]	N_{e^+}	Fraction	$\sigma_{stat.}$	$\sigma_{acc.}$	$\sigma_{sel.}$	$\sigma_{mig.}$	$\sigma_{ref.}$	$\sigma_{c.c.}$	$\sigma_{syst.}$
0.50–0.65	1242	0.0943	0.0027	0.0009	0.0034	0.0023	0.0003	0.0009	0.0043
0.65–0.81	5295	0.0917	0.0015	0.0008	0.0024	0.0020	0.0002	0.0008	0.0033
0.81–1.00	10 664	0.0862	0.0008	0.0007	0.0014	0.0018	0.0002	0.0007	0.0025
1.00–1.21	14 757	0.0820	0.0007	0.0006	0.0009	0.0016	0.0002	0.0006	0.0020
1.21–1.45	22 199	0.0775	0.0005	0.0005	0.0008	0.0014	0.0001	0.0005	0.0018
1.45–1.70	27 145	0.0724	0.0005	0.0004	0.0007	0.0013	0.0001	0.0004	0.0016
1.70–1.97	33 041	0.0686	0.0004	0.0003	0.0006	0.0011	0.0001	0.0003	0.0014
1.97–2.28	39 475	0.0650	0.0003	0.0002	0.0006	0.0010	0.0001	0.0003	0.0012
2.28–2.60	36 067	0.0622	0.0004	0.0002	0.0005	0.0008	0.0001	0.0002	0.0010
2.60–2.94	35 442	0.0597	0.0003	0.0001	0.0004	0.0007	0.0001	0.0002	0.0009
2.94–3.30	34 977	0.0576	0.0003	0.0001	0.0003	0.0006	0.0001	0.0002	0.0008
3.30–3.70	31 762	0.0559	0.0003	0.0001	0.0003	0.0006	0.0001	0.0002	0.0007
3.70–4.11	33 051	0.0553	0.0003	0.0001	0.0002	0.0005	0.0001	0.0002	0.0006
4.11–4.54	30 310	0.0539	0.0003	0.0001	0.0001	0.0004	0.0001	0.0002	0.0005
4.54–5.00	29 764	0.0528	0.0003	0.0001	0.0001	0.0003	0.0001	0.0002	0.0004
5.00–5.50	27 688	0.0524	0.0003	0.0001	0.0001	0.0003	0.0001	0.0002	0.0004
5.50–6.00	23 488	0.0515	0.0003	0.0001	0.0001	0.0002	0.0001	0.0002	0.0003
6.00–6.56	22 113	0.0514	0.0003	0.0001	0.0001	0.0002	0.0001	0.0002	0.0003
6.56–7.16	20 863	0.0511	0.0004	0.0001	0.0001	0.0001	0.0001	0.0002	0.0003
7.16–7.80	18 033	0.0506	0.0004	0.0001	0.0001	0.0001	0.0001	0.0002	0.0003
7.80–8.50	15 719	0.0509	0.0004	0.0001	0.0001	0.0001	0.0001	0.0002	0.0003
8.50–9.21	13 389	0.0514	0.0004	0.0001	0.0001	0.0001	0.0001	0.0002	0.0003
9.21–9.95	12 245	0.0513	0.0005	0.0001	0.0001	0.0001	0.0001	0.0002	0.0003
09.95–10.73	10 641	0.0523	0.0005	0.0001	0.0001	0.0002	0.0001	0.0002	0.0003
10.73–11.54	9504	0.0532	0.0006	0.0001	0.0001	0.0002	0.0001	0.0002	0.0003
11.54–12.39	7846	0.0546	0.0006	0.0001	0.0001	0.0002	0.0001	0.0002	0.0003
12.39–13.27	7646	0.0553	0.0006	0.0001	0.0001	0.0002	0.0001	0.0002	0.0003
13.27–14.19	6457	0.0552	0.0007	0.0001	0.0001	0.0002	0.0001	0.0002	0.0004
14.19–15.15	5704	0.0558	0.0007	0.0001	0.0001	0.0002	0.0001	0.0002	0.0004
15.15–16.15	5419	0.0570	0.0008	0.0001	0.0001	0.0003	0.0001	0.0002	0.0004
16.15–17.18	4689	0.0585	0.0009	0.0001	0.0001	0.0003	0.0001	0.0002	0.0004
17.18–18.25	4016	0.0601	0.0010	0.0001	0.0001	0.0003	0.0001	0.0002	0.0004
18.25–19.37	3906	0.0596	0.0010	0.0001	0.0001	0.0003	0.0001	0.0002	0.0004
19.37–20.54	3777	0.0625	0.0010	0.0001	0.0001	0.0003	0.0001	0.0002	0.0004
20.54–21.76	3244	0.0617	0.0011	0.0001	0.0001	0.0004	0.0001	0.0002	0.0005
21.76–23.07	2910	0.0640	0.0012	0.0001	0.0001	0.0004	0.0001	0.0002	0.0005
23.07–24.45	2813	0.0655	0.0013	0.0001	0.0002	0.0004	0.0001	0.0002	0.0005
24.45–25.87	2631	0.0652	0.0013	0.0001	0.0002	0.0004	0.0001	0.0002	0.0005
25.87–27.34	2397	0.0662	0.0014	0.0001	0.0002	0.0004	0.0001	0.0002	0.0005
27.34–28.87	2325	0.0704	0.0015	0.0001	0.0002	0.0005	0.0001	0.0002	0.0006
28.87–30.45	2040	0.0717	0.0016	0.0001	0.0002	0.0005	0.0001	0.0002	0.0006
30.45–32.10	1706	0.0719	0.0018	0.0001	0.0003	0.0005	0.0001	0.0002	0.0006
32.10–33.80	1530	0.0721	0.0019	0.0001	0.0003	0.0005	0.0001	0.0002	0.0006
33.80–35.57	1496	0.0766	0.0021	0.0001	0.0003	0.0005	0.0001	0.0002	0.0007
35.57–37.40	1327	0.0732	0.0021	0.0001	0.0003	0.0005	0.0001	0.0002	0.0007
37.40–40.00	1607	0.0781	0.0020	0.0001	0.0004	0.0006	0.0001	0.0002	0.0007
40.00–43.39	1616	0.0806	0.0021	0.0001	0.0004	0.0006	0.0001	0.0002	0.0008
43.39–47.01	1401	0.0872	0.0024	0.0001	0.0005	0.0006	0.0001	0.0003	0.0008
47.01–50.87	1116	0.0840	0.0027	0.0002	0.0005	0.0006	0.0001	0.0003	0.0009
50.87–54.98	1041	0.0887	0.0028	0.0002	0.0006	0.0007	0.0001	0.0003	0.0010
54.98–59.36	837	0.0921	0.0032	0.0002	0.0007	0.0007	0.0001	0.0004	0.0010
59.36–64.03	710	0.0933	0.0037	0.0002	0.0007	0.0007	0.0001	0.0004	0.0011
64.03–69.00	644	0.0974	0.0039	0.0002	0.0008	0.0007	0.0002	0.0005	0.0012
69.00–74.30	606	0.1069	0.0044	0.0002	0.0009	0.0007	0.0002	0.0006	0.0013

(Table continued)

TABLE I. (*Continued*).

Energy [GeV]	N_{e^+}	Fraction	$\sigma_{stat.}$	$\sigma_{acc.}$	$\sigma_{sel.}$	$\sigma_{mig.}$	$\sigma_{ref.}$	$\sigma_{c.c.}$	$\sigma_{syst.}$
74.30–80.00	450	0.0963	0.0047	0.0002	0.0010	0.0007	0.0002	0.0006	0.0014
80.00–86.00	381	0.1034	0.0056	0.0002	0.0011	0.0007	0.0002	0.0007	0.0015
86.00–92.50	398	0.1207	0.0063	0.0002	0.0011	0.0007	0.0003	0.0009	0.0016
92.50–100.0	358	0.1169	0.0063	0.0002	0.0013	0.0007	0.0003	0.0010	0.0018
100.0–115.1	524	0.1205	0.0054	0.0002	0.0014	0.0007	0.0004	0.0013	0.0021
115.1–132.1	365	0.1110	0.0062	0.0002	0.0017	0.0007	0.0005	0.0018	0.0026
132.1–151.5	271	0.1327	0.0083	0.0002	0.0020	0.0007	0.0006	0.0024	0.0032
151.5–173.5	228	0.1374	0.0097	0.0002	0.0023	0.0007	0.0007	0.0031	0.0040
173.5–206.0	225	0.1521	0.0109	0.0002	0.0027	0.0007	0.0008	0.0044	0.0053
206.0–260.0	178	0.1550	0.0124	0.0003	0.0034	0.0007	0.0011	0.0076	0.0084
260.0–350.0	135	0.1590	0.0168	0.0003	0.0045	0.0007	0.0015	0.0123	0.0132
350.0–500.0	72	0.1471	0.0278	0.0003	0.0064	0.0007	0.0022	0.0182	0.0194

top of the AMS detector. The contribution of individual sources to the systematic error are added in quadrature to arrive at the total systematic uncertainty.

Most importantly, several independent analyses were performed on the same data sample by different study groups. Results of these analyses are consistent with those presented in this Letter.

Figure 2 shows the behavior of the positron fraction at low energies, from 1 to 35 GeV. As seen, below ~8 GeV, the positron fraction decreases rapidly as expected from the diffuse production of positrons [16]. Then the fraction begins to increase steadily with energy. The AMS data provide accurate information on the minimum of the positron fraction.

Our earlier result [2], in which we observed the increase of the positron fraction with decreasing slope above 20 GeV, is consistent with this new measurement. The increase of the positron fraction has been reported by earlier experiments: TS93 [17], Wizard/CAPRICE [18], HEAT [19], AMS-01 [20], PAMELA [21], and Fermi-LAT [22].

The new result extends the energy range to 500 GeV and is based on a significant increase in the statistics by a factor of 1.7. Figure 3 explores the behavior of the positron fraction at high energies (> 10 GeV) and compares it with earlier measurements. We observe that above ~200 GeV the positron fraction is no longer increasing with energy.

To examine the energy dependence of the positron fraction quantitatively in a model independent way, straight line fits were performed over the entire energy range with a sliding energy window, where the width of the window varies with energy to have sufficient sensitivity to the slope. Each window covers about eight bins, at energies above 200 GeV it covers three bins. The variation of the slope of the positron fraction from 4 GeV upwards is shown in Fig. 4(a). As seen in the figure, above 30 GeV the slope decreases logarithmically with energy. Fitting the change of the slope as a function of energy above 30 GeV with a two parameter fit [slope $= c\log(E/E_0)$ where c is the normalization and E_0 is the energy at which the slope crosses zero, that is, the energy at which the positron fraction reaches its maximum] results in a determination of $E_0 = 275 \pm 32$ GeV with a $\chi^2/\text{d.f.} = 3.9/12$ taking into account correlations. The result of the fit is shown as a solid line in Fig. 4(a). This confirms our observation from Fig. 3 that above ~200 GeV the positron fraction is no longer increasing with energy. The exact value of E_0, which is an important parameter in understanding the physics of the positron fraction [3], will be determined accurately with more data and by extending the energy range.

This is the first experimental evidence of the existence of a new behavior of the positron fraction at high energy.

We present a fit to the data of a minimal model, described in our previous Letter [2]. In this model the e^+ and e^- fluxes are parametrized as the sum of its individual diffuse power law spectrum and a common source term with an exponential cutoff parameter, E_s

$$\Phi_{e^+} = C_{e^+}E^{-\gamma_{e^+}} + C_s E^{-\gamma_s} e^{-E/E_s}; \quad (1)$$

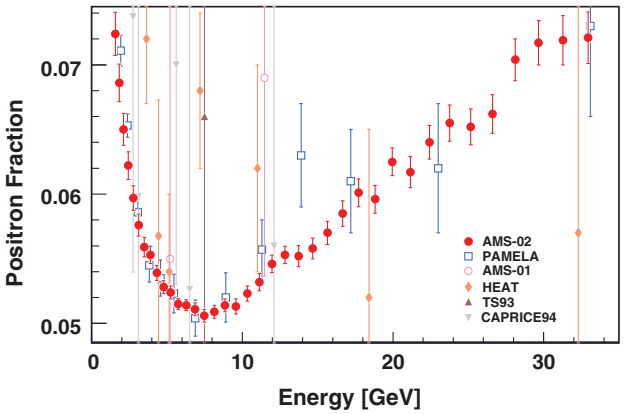

FIG. 2 (color). The positron fraction from 1 to 35 GeV. It shows a rapid decrease from 1 to ~8 GeV followed by a steady increase. The AMS data provide accurate information on the minimum of the positron fraction.

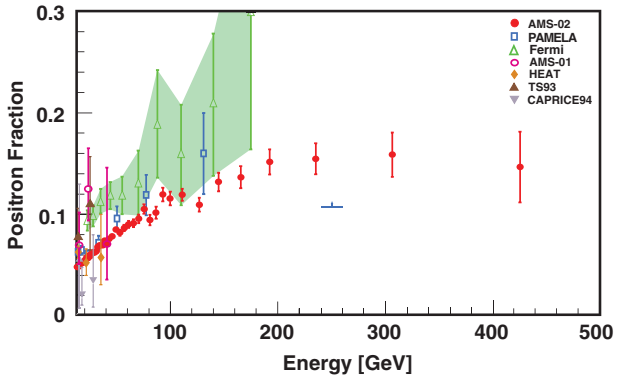

FIG. 3 (color). The positron fraction above 10 GeV, where it begins to increase. The present measurement extends the energy range to 500 GeV and demonstrates that, above ~200 GeV, the positron fraction is no longer increasing. Measurements from PAMELA [21] (the horizontal blue line is their lower limit), Fermi-LAT [22], and other experiments [17–20] are also shown.

$$\Phi_{e^-} = C_{e^-} E^{-\gamma_{e^-}} + C_s E^{-\gamma_s} e^{-E/E_s}, \qquad (2)$$

(with E in GeV). A fit of this model to the data with their total errors (the quadratic sum of the statistical and systematic errors) in the energy range from 1 to 500 GeV yields a $\chi^2/\text{d.f.} = 36.4/58$ and the cutoff parameter $1/E_s = 1.84 \pm 0.58$ TeV^{-1} with the other parameters having similar values to those in [2], $C_{e^+}/C_{e^-} = 0.091 \pm 0.001$, $C_s/C_{e^-} = 0.0061 \pm 0.0009$, $\gamma_{e^-} - \gamma_{e^+} = -0.56 \pm 0.03$, and $\gamma_{e^-} - \gamma_s = 0.72 \pm 0.04$. (The same model with no exponential cutoff parameter, i.e., $1/E_s$ set to 0, is excluded at the 99.9% C.L. when fit to the data.) The resulting fit is shown in Fig. 4(b) as a solid curve together with the 68% C.L. range of the fit parameters. No fine structures are observed in the data. In our previous Letter, we reported that solar modulation has no observable effect on our measured positron fraction, and this continues to be the case.

An analysis of the arrival directions of positrons and electrons was presented in [2]. The same analysis was performed including the additional data. The positron to electron ratio remains consistent with isotropy; the upper limit on the amplitude of the dipole anisotropy is $\delta \leq 0.030$ at the 95% C. L. for energies above 16 GeV.

Following the publication of our first Letter [2], there have been many interesting interpretations [3] with two popular classes. In the first, the excess of e^+ comes from pulsars. In this case, after flattening out with energy, the positron fraction will begin to slowly decrease and a dipole anisotropy should be observed. In the second, the shape of the positron fraction is due to dark matter collisions. In this case, after flattening out, the fraction will decrease rapidly with energy due to the finite and specific mass of the dark matter particle, and no dipole anisotropy will be observed. Over its lifetime, AMS will reach a dipole anisotropy sensitivity of $\delta \simeq 0.01$ at the 95% C.L.

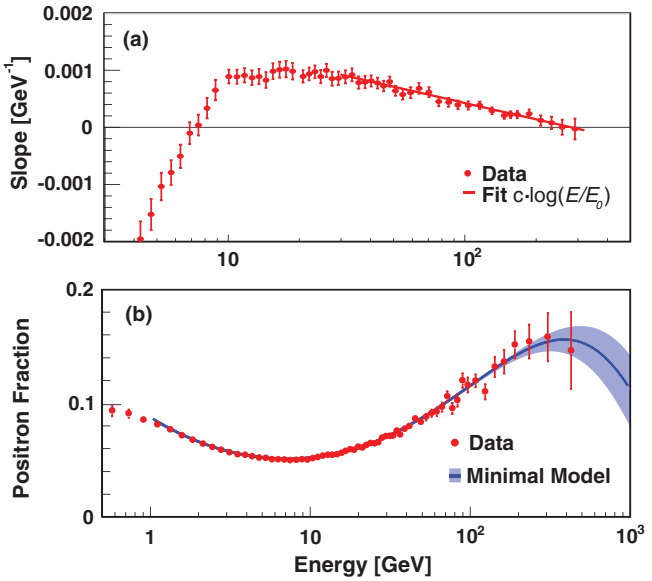

FIG. 4 (color). (a) The slope of the positron fraction vs energy over the entire energy range (the values of the slope below 4 GeV are off scale). The line is a logarithmic fit to the data above 30 GeV. (b) The positron fraction measured by AMS and the fit of a minimal model (solid curve, see text) and the 68% C.L. range of the fit parameters (shaded). For this fit, both the data and the model are integrated over the bin width. The error bars are the quadratic sum of the statistical and systematic uncertainties. Horizontally, the points are placed at the center of each bin.

The new measurement shows a previously unobserved behavior of the positron fraction. The origin of this behavior can only be ascertained by continuing to collect data up to the TeV region and by measuring the antiproton to proton ratio to high energies. These are among the main goals of AMS.

In conclusion, the 10.9×10^6 primary positron and electron events collected by AMS on the ISS show that, above ~200 GeV, the positron fraction no longer exhibits an increase with energy. This is a major change in the behavior of the positron fraction.

We thank former NASA Administrator Daniel S. Goldin for his dedication to the legacy of the ISS as a scientific laboratory and his decision for NASA to fly AMS as a DOE payload. We also acknowledge the continuous support of the NASA leadership including Charles Bolden, William Gerstenmeier, and Mark Sistilli. AMS is a U.S. DOE sponsored international collaboration. We are grateful for the support of Jim Siegrist, Michael Salamon, Dennis Kovar, Robin Staffin, Saul Gonzalez, and John O'Fallon of the DOE. We also acknowledge the continuous support from M.I.T. and its School of Science, Michael Sipser, Marc Kastner, Ernest Moniz, Edmund Bertschinger, and Richard Milner. We acknowledge support from: CAS, NNSF, MOST, NLAA, and the provincial governments of Shandong, Jiangsu, and Guangdong, China; CNRS, IN2P3, CNES, Enigmass, and the ANR, France, and

Bernard Accoyer, former President of the French National Assembly; DLR, P. Hintze, J. Trümper, and J. D. Woerner, Germany; INFN, E. Iarocci, R. Petronzio, and F. Ferroni, and ASI, S. De Julio, S. Vetrella, G. Bignami, and E. Saggese, Italy; CIEMAT, CDTI, SEIDI–MINECO, and CPAN, Spain; the Swiss National Science Foundation (SNSF), federal and cantonal authorities, Switzerland; and Academia Sinica and the National Science Council (NSC), former President of Academia Sinica Yuan-Tseh Lee and former Ministers of NSC, Chien-Jen Chen, Maw-Kuen Wu, and Luo-Chuan Lee, Taiwan. We gratefully acknowledge the strong support from CERN: Rolf-Dieter Heuer, Robert Aymar, Luciano Maiani, as well as Steve Meyers and Andrzej Siemko. From ESA, we thank Jean-Jacques Dordain, Simona Di Pippo, and Martin Zell for their support. We are grateful for important discussions with Barry Barish, Claude Canizares, James Cronin, Jonathan Ellis, Len Fisk, Sheldon Glashow, Alan Guth, Neal Lane, Steve Olsen, Álvaro de Rújula, George Smoot, Jian Song, Evgeny Velikhov, Steven Weinberg, Frank Wilczek, and Cunhao Zhang. We are most grateful for the strong support of the flight control teams at Johnson Space Center, Houston, and Marshall Space Flight Center, Huntsville, which has allowed AMS to operate continuously on the ISS for over three years.

[a]Present address: ISDC, CH–1290 Versoix, Switzerland.
[b]Present address: ASI, Rome, I–00133, Italy
[c]Work carried out at the ASI Science Data Center (ASDC) in the framework of the ASI–INFN agreement C/011/11/1.
[d]Present address: LLNL, Livermore, CA 94550.
[e]Deceased.
[f]Also at Xi'an Jiaotong University, XJTU, Xi'an, 710049, China; and China Scholarship Council.
[g]Also at Sun Yat–Sen University, SYSU, Guangzhou, 510275, China; and China Scholarship Council.
[h]Present address: SRON, NL–3584 Utrecht, Netherlands.
[i]Present address: UNC CB 3255, Chapel Hill, NC 27599.
[j]Present address: European Organization for Nuclear Research, CERN, CH–1211 Geneva 23, Switzerland.
[k]Also at Shandong University, SDU, Jinan, Shandong, 250100, China; and China Scholarship Council.
[l]Also at Harbin Institute of Technology, HIT, Harbin, 150001, China; and China Scholarship Council.
[m]Also at University of Science and Technology of China, USTC, Hefei, 230026, China; and China Scholarship Council.
[n]Present address: UC Santa Barbara, Santa Barbara, CA 93106.
[o]Also at Università di Siena, I–53100 Siena, Italy.
[p]Present address: U. Washington, Seattle, WA 98195.
[q]Also at Beijing Normal University, BNU, Beijing, 100875, China; and China Scholarship Council.
[r]Also at Southeast University, SEU, Nanjing, 210096, China; and China Scholarship Council.
[s]Supported by the Centre national d'études spatiales, CNES.
[t]Present address: ORACLE, Redwood City, CA 94065.
[u]Supported by the Deutsches Zentrum für Luft– und Raumfahrt, DLR.; Computing resources from JARA-HPC under Project No. JARA0052.
[v]Supported by the Turkish Atomic Energy Authority, TAEK.
[w]Supported by the National Natural Science Foundation of China.
[x]Also supported by the Italian Space Agency, ASI, Contract No. ASI-INFN I/002/13/0.
[y]Also supported by the Ministry of Science and Technology.
[z]Grants No. NRF-2009-0080142 and No. NRF-2012-010226.
[A]Computing resources from JARA-HPC under Project No. JARA0052.
[B]Supported by the Deutsches Zentrum für Luft- und Raumfahrt, DLR.
[C]Also supported by SEIDI and CPAN.
[D]Supported by Consejo Nacional de Ciencia y Tecnología, CONACYT.
[E]Grant No. NRF-2013-004883.

[1] M. S. Turner and F. Wilczek, Phys. Rev. D **42**, 1001 (1990); J. Ellis, in *Proceedings of the 26th International Cosmic Ray Conference: Salt Lake City, Utah, August, 1999* (World Scientific, Singapore, 1999); H. C. Cheng, J. L. Feng, and K. T. Matchev, Phys. Rev. Lett. **89**, 211301 (2002); S. Profumo and P. Ullio, J. Cosmol. Astropart. Phys. 07 (2004) 006; D. Hooper and J. Silk, Phys. Rev. D **71**, 083503 (2005); E. Ponton and L. Randall, J. High Energy Phys. 04 (2009) 080; G. Kane, R. Lu, and S. Watson, Phys. Lett. B **681**, 151 (2009); D. Hooper, P. Blasi, and P. D. Serpico, J. Cosmol. Astropart. Phys. 01 (2009) 025; Y.-Z. Fan, B. Zhang, and J. Chang, Int. J. Mod. Phys. D **19**, 2011 (2010); M. Pato, M. Lattanzi, and G. Bertone, J. Cosmol. Astropart. Phys. 12 (2010) 020.

[2] M. Aguilar *et al.*, Phys. Rev. Lett. **110**, 141102 (2013).

[3] There are many recent excellent theoretical articles on the positron fraction. A few examples are L. Feng, R.-Z. Yang, H.-N. He, T.-K. Dong, Y.-Z. Fan, and J. Chang, Phys. Lett. B **728**, 250 (2014); K. Blum, B. Katz, and E. Waxman, Phys. Rev. Lett. **111**, 211101 (2013); L. Bergström, T. Bringmann, I. Cholis, D. Hooper, and C. Weniger, Phys. Rev. Lett. **111**, 171101 (2013); J. Kopp, Phys. Rev. D **88**, 076013 (2013); I. Cholis and D. Hooper, Phys. Rev. D **88**, 023013 (2013); T. Linden and S. Profumo, Astrophys. J. **772**, 18 (2013). Cholis, Kopp (private communication).

[4] A. Kounine, Int. J. Mod. Phys. E **21**, 1230005 (2012); S. C. C. Ting, Nucl. Phys. B, Proc. Suppl. **243–244**, 12 (2013). S. C. Lee, in *Proceedings or the 20th International Conference on Supersymmetry and Unification of Fundamental Interactions (SUSY 2012), Beijing, China, 2012* (unpublished); M. Aguilar, in *Proceedings of the XL International Meeting on Fundamental Physics, Centro de Ciencias de Benasque Pedro Pascual, Benasque, 2012* (unpublished); S. Schael, in *Proceedings of the 10th Symposium on Sources and Detection of Dark Matter and Dark Energy in the Universe, Los Angeles, 2012* (unpublished); B. Bertucci, *Proc. Sci.*, EPS-HEP (2011) 67; M. Incagli, AIP Conf. Proc. **1223**, 43 (2009);

R. Battiston, Nucl. Instrum. Methods Phys. Res., Sect. A **588**, 227 (2008).

[5] B. Alpat *et al.*, Nucl. Instrum. Methods Phys. Res., Sect. A **613**, 207 (2010).

[6] T. Kirn, Nucl. Instrum. Methods Phys. Res., Sect. A **706**, 43 (2013); P. Doetinchem *et al.*, Nucl. Instrum. Methods Phys. Res., Sect. A **558**, 526 (2006); F. Hauler *et al.*, IEEE Trans. Nucl. Sci. **51**, 1365 (2004).

[7] V. Bindi *et al.*, Nucl. Instrum. Methods Phys. Res., Sect. A **743**, 22 (2014); A. Basili, V. Bindi, D. Casadei, G. Castellini, A. Contin, A. Kounine, M. Lolli, F. Palmonari, and L. Quadrani, Nucl. Instrum. Methods Phys. Res., Sect. A **707**, 99 (2013); V. Bindi *et al.*, Nucl. Instrum. Methods Phys. Res., Sect. A **623**, 968 (2010).

[8] K. Luebelsmeyer *et al.*, Nucl. Instrum. Methods Phys. Res., Sect. A **654**, 639 (2011); M. Aguilar *et al.*, Phys. Rep. **366**, 331 (2002).

[9] Ph. von Doetinchem, W. Karpinski, Th. Kirn, K. Lübelsmeyer, St. Schael, and M. Wlochal, Nucl. Phys. B, Proc. Suppl. **B197**, 15 (2009).

[10] M. Aguilar-Benitez *et al.*, Nucl. Instrum. Methods Phys. Res., Sect. A **614**, 237 (2010); in *Proceedings of the 30th International Cosmic Ray Conference: Merida, Yucataán, Mexico, 2007* (Karlsruhe, FZKA, 2007); P. Aguayo *et al.*, Nucl. Instrum. Methods Phys. Res., Sect. A **560**, 291 (2006); B. Baret *et al.*, Nucl. Instrum. Methods Phys. Res., Sect. A **525**, 126 (2004); J. Casaus, Nucl. Phys. B, Proc. Suppl. **113**, 147 (2002).

[11] C. Adloff *et al.*, Nucl. Instrum. Methods Phys. Res., Sect. A **714**, 147 (2013).

[12] B. P. Roe, H.-J. Yang, J. Zhu, Y. Liu, I. Stancu, and G. McGregor, Nucl. Instrum. Methods Phys. Res., Sect. A **543**, 577 (2005).

[13] J. Allison *et al.*, IEEE Trans. Nucl. Sci. **53**, 270 (2006); S. Agostinelli *et al.*, Nucl. Instrum. Methods Phys. Res., Sect. A **506**, 250 (2003).

[14] J. Alcaraz *et al.*, Phys. Lett. B **484**, 10 (2000).

[15] C. Størmer, *The Polar Aurora* (Oxford University Press, London, 1950).

[16] P. D. Serpico, Astropart. Phys. **39–40**, 2 (2012); T. Delahaye, R. Lineros, F. Donato, N. Fornengo, J. Lavalle, P. Salati, and R. Taillet, Astron. Astrophys. **501**, 821 (2009); I. V. Moskalenko and A. W. Strong, Astrophys. J. **493**, 694 (1998). We have not included the model predictions as their uncertainty, $\boldsymbol{O}(20\%)$, is larger than our errors. Moskalenko (private communication).

[17] R. Golden *et al.*, Astrophys. J. **457**, L103 (1996).

[18] M. Boezio *et al.*, Adv. Space Res. **27**, 669 (2001).

[19] J. J. Beatty *et al.*, Phys. Rev. Lett. **93**, 241102 (2004); M. A. DuVernois *et al.*, Astrophys. J. **559**, 296 (2001).

[20] M. Aguilar *et al.*, Phys. Lett. B **646**, 145 (2007).

[21] O. Adriani *et al.*, Phys. Rev. Lett. **111**, 081102 (2013); Astropart. Phys. **34**, 1 (2010); Nature (London) **458**, 607 (2009).

[22] M. Ackermann *et al.*, Phys. Rev. Lett. **108**, 011103 (2012).